01 Jan 2023

Temperature Dependence Of The Electronic Absorption Spectrum Of NO2

Steve Ndengué

Ernesto Quintas Sánchez
Missouri University of Science and Technology, quintassancheze@mst.edu

Richard Dawes
Missouri University of Science and Technology, dawesr@mst.edu

Christopher C. Blackstone

et. al. For a complete list of authors, see https://scholarsmine.mst.edu/chem_facwork/3642

Recommended Citation

S. Ndengué et al., "Temperature Dependence Of The Electronic Absorption Spectrum Of NO2," *Journal of Physical Chemistry A*, American Chemical Society, Jan 2023.
The definitive version is available at https://doi.org/10.1021/acs.jpca.3c02832

THE JOURNAL OF PHYSICAL CHEMISTRY A
A JOURNAL OF THE AMERICAN CHEMICAL SOCIETY

pubs.acs.org/JPCA

Article

Temperature Dependence of the Electronic Absorption Spectrum of NO_2

Steve Ndengué, Ernesto Quintas-Sánchez, Richard Dawes,* Christopher C. Blackstone, and David L. Osborn*

Cite This: *J. Phys. Chem. A* 2023, 127, 6051−6062

Read Online

ACCESS | Metrics & More | Article Recommendations | Supporting Information

ABSTRACT: The nitrogen dioxide (NO_2) radical is composed of the two most abundant elements in the atmosphere, where it can be formed in a variety of ways including combustion, detonation of energetic materials, and lightning. Relevant also to smog and ozone cycles, together these processes span a wide range of temperatures. Remarkably, high-resolution NO_2 electronic absorption spectra have only been reported in a narrow range below about 300 K. Previously, we reported [*J. Phys. Chem. A* **2021**, *125*, 5519−5533] the construction of quasi-diabatic potential energy surfaces (PESs) for the lowest four electronic states ($\tilde{X}$, $\tilde{A}$, $\tilde{B}$, and $\tilde{C}$) of NO_2. In addition to three-dimensional PESs based on explicitly correlated MRCI(Q)-F12/VTZ-F12 *ab initio* data, the geometry dependence of each component of the dipoles and transition dipoles was also mapped into fitted surfaces. The multiconfigurational time-dependent Hartree (MCTDH) method was then used to compute the 0 K electronic absorption spectrum (from the ground rovibrational initial state) employing those energy and transition dipole surfaces. Here, in an extension of that work, we report an investigation into the effects of elevated temperature on the spectrum, considering the effects of the population of rotationally and vibrationally excited initial states. The calculations are complemented by new experimental measurements. Spectral contributions from hundreds of rotational states up to N = 20 and from 200 individually-characterized vibrational states were computed. A spectral simulation tool was developed that enables modeling the spectrum at various temperatures—by weighting individual spectral contributions via the partition function, or for pure excited initial states, which can be probed via transient absorption spectroscopy. We validate these results against experimental absorption spectroscopy data at high temperatures, as well as via a new measurement from the (1,0,1) initial vibrational state.

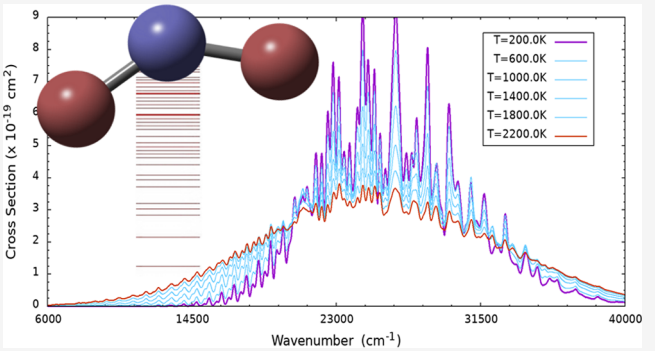

INTRODUCTION

In order to gain insight into the electronic absorption spectrum of NO_2, we recently reported 0 K simulations[1] based on full-dimensional (3D) potential energy surfaces (PESs) for the lowest four doublet electronic states ($\tilde{X}$, $\tilde{A}$, $\tilde{B}$, and $\tilde{C}$) of NO_2, calculated at the MRCI(Q)-F12/VTZ-F12 level. To treat electronic-state couplings, a properties-based diabatization scheme was used to determine (quasi)-diabatic PESs and coupling surfaces, and a neural network (NN)-based method was used to fit each element of the resulting potential energy matrices (PEMs). Each component of the dipole moment of each state and the transition dipole moments between them were fit into fully geometry-dependent surfaces. A total of 19 individual—energy, coupling, dipole, and transition dipole—surfaces were constructed. The multiconfigurational time-dependent Hartree (MCTDH) method was employed to compute rovibrational levels and predict the 0 K electronic absorption spectrum, complete with predicted absolute intensity. As shown in Figure 1, the total spectrum is separated into the main contribution to the cross section: the transition from the ground $\tilde{X}$ state to the excited $\tilde{A}$ state, and the more minor contribution from the transition to the coupled pair of $\tilde{B}$/$\tilde{C}$ states. The computed spectrum has not been scaled or shifted along either axis when compared to experiment in Figure 1. For the 0 K simulation, only the lowest rovibrational state was initially populated.

Our goal is to create a first-principles prediction without adjustable parameters of NO_2's absorption cross section, validated over a wide temperature range to experimental data. Here, we validate our computations to published and new experimental measurements presented in this work. Our approach to understanding temperature effects is twofold. First, we explore the effect of the significant rotational excitation

Received: April 29, 2023
Revised: June 8, 2023
Published: June 29, 2023

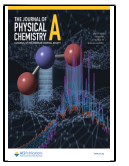

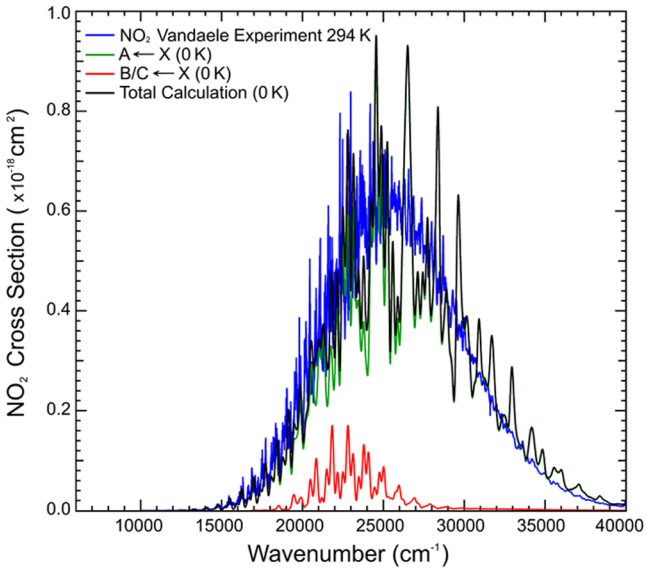

Figure 1. Electronic absorption spectrum of NO_2 calculated at 0 K by modeling excitation from the ground rovibrational state[1] is compared with the experimental measurement of Vandaele et al. from 1998.[2] The separate $\tilde{A} \leftarrow \tilde{X}$, $\tilde{B}/\tilde{C} \leftarrow \tilde{X}$, and total predicted spectrum (green, red, and black traces, respectively) are compared with the experiment (blue trace).

that occurs even at modest temperatures. Second, we explore the effects of vibrationally excited initial states, which are thermally populated at high temperatures or may be populated via the absorption of an infrared photon in a transient absorption experiment. The approach employed is to compute individual spectral contributions for each relevant initial state (whether populated thermally or otherwise). The partition function is evaluated by direct summation over the levels and can be used for the Boltzmann weighting of initial states. Such a comprehensive first-principles approach should enable the prediction of absorption cross sections at high temperatures needed for combustion and energetic materials applications, where experiments are challenging.

This paper is organized as follows. In the Methods Section, we describe the MCTDH-based approach to compute the hundreds of initial states—rotationally and vibrationally excited—used to determine their individual contributions to the simulated electronic spectra. We present an interactive spectral simulation software tool that can be used to make comparisons and plot predictions at various temperatures. We also describe our infrared pump, broadband probe apparatus to measure the transient absorption spectrum following excitation of the (1,0,1) vibrational level, which would be significantly populated at high temperatures. In the Results and Discussion Section, we assess the accuracy and character of the rovibrational states, which depend on the previously generated fitted surfaces and the underlying electronic structure method. The various effects of temperature on the electronic absorption spectrum are discussed and compared to a previously reported model and published high-temperature experimental absorption spectra. The dramatic effect of mode-specific initial state excitation is explored via predictions and valided by some new measurements. In the Conclusions and Outlook Section, we summarize the insights gained and discuss future plans for extensions of this work.

METHODS

As mentioned earlier, the MCTDH method[3,4] is the quantum dynamical approach used to perform the calculations—not only to obtain the rotational and vibrational states of the ground electronic state but also to compute the absorption spectra starting from those various initial states. The MCTDH methodology uses a relatively compact time-dependent variationally optimized single-particle functions (SPFs) basis set, which itself is expanded in a much larger time-independent Primitive Basis spanning the Hilbert space of the system. As mentioned in our previous work,[1] the MCTDH method has been applied to similar studies in the past,[5−7] including the calculation of rovibrational states.[8,9] The crucial ingredients needed to employ the MCTDH methodology for a given system (as implemented in the Heidelberg MCTDH Package[10]) are the potential energy, coupling, and properties surfaces. As in our previous work, we represent the system using valence coordinates and take advantage of the `Potfit` algorithm[11,12] to process the Neural Network PESs and Transition Dipole Moment Surfaces into a Sum-Of-Product (SOP) form, which is very efficient for wavepacket propagation in the MCTDH formalism.

Vibrational Levels. In our previous publication, we described in detail the calculation of initial vibrational levels on the ground electronic state. Only a brief summary is given here. The calculations of the (N = 0) vibrational states of the system were done using the block improved relaxation approach[3,13−15] as implemented in the MCTDH package (neglecting electron spin and nuclear hyperfine interactions). Progressing 8−10 states at a time, we moved up the ladder and computed the lowest 200 vibrational states of this system, which extends the range of energies to about 10,200 cm^{-1} above the zero point energy (ZPE). The vibrational levels in this energy range have been well characterized experimentally[16] and are closely matched by the calculations. We use the conventional labels ν_1, ν_2, and ν_3 for the symmetric stretch, bend, and asymmetric stretch modes, respectively.[1,16] No discrepancies in assignments or missing levels were noted from either the tabulated experimental assignments or the corresponding calculations. The parameters of the primitive and the SPF basis sets used for these calculations are reported in Table 1.

Table 1. Parameters of the Primitive and SPF Basis Sets Used for the Vibrational Calculations on the Ground-State PES of NO_2[a]

coords.	primitive basis	number of points	range	size of SPF basis
r_1	sine	37	1.800−3.774	10−33
r_2	sine	37	1.800−3.774	10−33
θ	Leg/R	64	1.4−π	10−32

[a]'sine' stands for the sine DVR. 'Leg/R' is the restricted Legendre DVR. The units for distance and angle are Bohr and radian, respectively.

Rovibrational Excitation. For rovibrational levels on the spin-doublet ground $\tilde{X}$ electronic state, (integer) values of N represent the angular momentum of the nuclei, which combines with the electron spin to give the two half-integer magnetic levels $J = N \pm 1/2$. In this study, we neglect electron spin-rotation coupling so the total angular momentum J is approximated simply as the nuclear angular momentum (i.e., $J = N$). Thus, neglecting electron spin (and nuclear ^{14}N hyperfine splitting),

https://doi.org/10.1021/acs.jpca.3c02832
J. Phys. Chem. A 2023, 127, 6051−6062

we will refer to rotationally excited initial states in terms of an integer N.

The calculations of the rovibrational states ($N > 0$) were also done with the block improved relaxation approach, in a similar fashion to those with $N = 0$. Here, however, the Hamiltonian (and specifically the kinetic energy operator) as well as the primitive and SPF basis sets were extended to take into account the rotational contributions. The kinetic energy operator in the valence coordinates representation used in this work (with the inclusion of the total rotation of the system) has been developed and described in detail in other works.[17−19] In order to describe the rotational motion, we used the extended Legendre (KLeg) discrete variable representation (DVR)—instead of the restricted Legendre DVR used for the $N = 0$ calculation. The KLeg DVR uses the 2-dimensional spherical harmonic basis functions, with one degree of freedom taking into account the bending motion of the molecule. K is the projection of the angular momentum on the body-fixed z axis. The complete K range $[-N, N]$ was specified.[20,21] The extended Legendre DVR covers the full angular range of $\theta = 0-\pi$. However, part of this angular range is not accessible since the PES diverges for small angles as the two O-atoms impinge on each other. Thus, numerically, a high ceiling was imposed on the PES to exclude this domain, extending the physically relevant $1.4-\pi$ range accurately described by our PES. Spectroscopic and dynamics calculations for $N = 0$ were then carried out and compared with our previous results, showing that the ceiling did not affect the eigenenergies or the electronic absorption spectrum. The parameters of the primitive and the SPF basis sets used for these calculations are reported in Table 2.

Table 2. Parameters of the Primitive and SPF Basis Used for the Rovibrational Calculations on the Ground-State PES of NO_2[a]

coords.	primitive basis	number of points	range	size of SPF basis
r_1	sine	37	1.800−3.774	10−33
r_2	sine	37	1.800−3.774	10−33
θ	KLeg	64	$0.0-\pi$	10−32
k	K	40	−20−20	

[a]'sine' stands for the sine DVR. 'KLeg'/'K' is the extended Legendre DVR. The units for distance and angle are Bohr and radian, respectively.

Electronic Absorption Spectra. Calculation of the electronic absorption spectrum for a given initial rovibrational state followed a similar procedure to our previous work at 0 K on this system, for both the $\tilde{A} \leftarrow \tilde{X}$ and $\tilde{B}/\tilde{C} \leftarrow \tilde{X}$ components. The primitive bases for the $N = 0$ calculations are displayed in Table 1, and those for $N > 0$ are displayed in Table 2. However, one major impact of elevated temperatures on the spectrum is a spread of the absorption intensity, especially into the low-energy wing. For a moderate range of temperatures, the effect of temperature on the spectral envelope has been observed and modeled by Kirmse et al.,[22] which we will discuss in more detail in a later section. In order to better resolve and appreciate changes to the spectrum, especially approaching the baseline on the low-energy side, tighter convergence criteria were specified in the simulations. Specifically, we increase the accuracy of the integrators used in the time-dependent dynamics. For these simulations, we used a constant mean field (CMF) with an initial time step of 0.5 fs and a tolerance of 10^{-5}, coupled with a Short Iterative Lanczos (SIL) integrator for the A-vector with a maximal order of 15 and an accuracy of 10^{-6}, and a Bulirsch−Stoer (BS) extrapolation integrator for the SPFs with a maximal order of 8 and an accuracy of 10^{-6}. Similarly, to improve spectral convergence, in particular in the wings of the spectrum, the autocorrelation function was obtained every 0.1 fs—instead of the 0.5 fs employed in our previous work. The length of propagation, which dictates spectral resolution, was kept at 200 fs as was used previously. Tests confirmed that these specified parameters well converge all reported quantities.

Experimental Section. We conducted a transient absorption experiment to probe electronic absorption in NO_2 originating from the (1,0,1) vibrational overtone level. The experimental apparatus is described in Figure 2. An evacuated sample cell with a pathlength of 51.4 cm was filled with 0.974−1.057 Torr of NO_2. A broadband visible spectrum was collected using an SLS201L Stabilized Tungsten Light Source with an internal SRF11 filter to flatten the spectral profile. The white light propagated along the centerline of the cell, was dispersed in an Andor Kymera 193i spectrometer by an 800 nm blaze grating and detected with an Andor DH434-FO CCD camera gated by a fiber-coupled microchannel plate (MCP). NO_2 was excited to the (1,0,1) level by a LaserVision optical parametric oscillator (OPO-A) with a 3.6 cm^{-1} bandwidth centered at 2918.2 cm^{-1}, which coincides with the maximum absorption in the R-branch of the (1,0,1) band. The OPO radiation is aligned colinear to the continuous white light path using two dichroic mirrors. A KG-1 filter protects the spectrometer from stray infrared radiation. The OPO was triggered 54 ns before the start of the 1 s wide MCP gate in order to maximize observation time while minimizing the effect of collisions that remove the population from the (1,0,1) level. We collected spectra alternately with the OPO blocked and unblocked, providing the 294 K reference and the OPO-modified electronic absorption spectra, from which we extract a difference spectrum. Additional details of the experiment and its analysis are provided in the Supporting Information (SI).

Spectral Simulation Tool. In simulations using our approach for a molecule such as NO_2, once all of the energies, couplings, and properties are accurately computed, diabatized, and fitted into convenient representations, a large number of quantum dynamics simulations are typically performed. Here, more than 500 individual predicted absorption spectra were computed, each one the output of a time-dependent wavepacket calculation performed using the MCTDH method, initiated from different individual rovibrational states of the $\tilde{X}$ electronic state. The impact of thermal or nonthermal excitation on the predicted spectrum was assessed by wavepacket propagation from the lowest 200 vibrational levels of the $\tilde{X}$ state (all with $N = 0$), and separately, exploring the effect of rotational excitation by considering more than 300 rotationally excited levels up to $N = 20$ for the (0,0,0) vibrational level. We developed a Spectral Simulation Tool to manage and archive the data, as well as to facilitate analyses and comparisons with experiments. The tool contains all of the computed data as well as available experimental data, and thermodynamic vibrational and rotational partition functions are constructed by explicit state counting. Thus, plots showing individual or aggregate contributions to spectra (for a single or a sequence of temperatures) can be easily generated and compared with experiments. Boltzmann weighting can be applied to spectral contributions from hundreds of initial states to predict the spectrum at any chosen temperature. In addition to equilibrium

https://doi.org/10.1021/acs.jpca.3c02832
J. Phys. Chem. A 2023, 127, 6051−6062

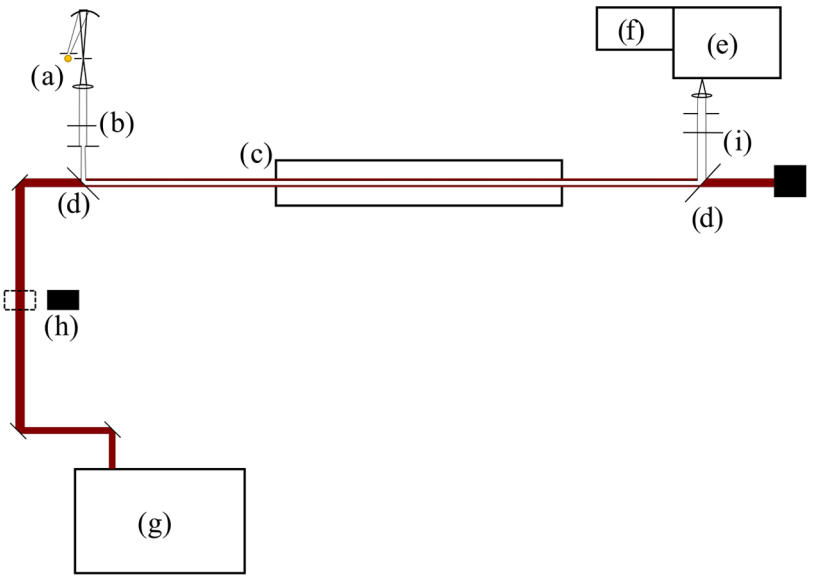

Figure 2. Schematic of the experiment. The continuous broadband white light (a) is collimated by a concave spherical mirror and a biconvex lens, both of 200 mm focal length. Light was attenuated by an iris at the focal point of the 200 mm mirror, and again by a second iris after the collimating lens to match the white light cross section to the OPO cross section. A 400 nm long-pass filter (b) was used to eliminate the possibility of photodissociation of NO_2. The white light was directed to the 51.4 cm pathlength sample cell (c) by a custom dichroic mirror (d) (Lattice Electro Optics). A second dichroic directed the white light toward the spectrometer (e) and camera (f). Protected silver mirrors reflected the OPO (g) beam to the sample cell. The OPO may be blocked or unblocked (h) during acquisition. A KG-1 filter (i) protected the spectrometer from stray infrared radiation.

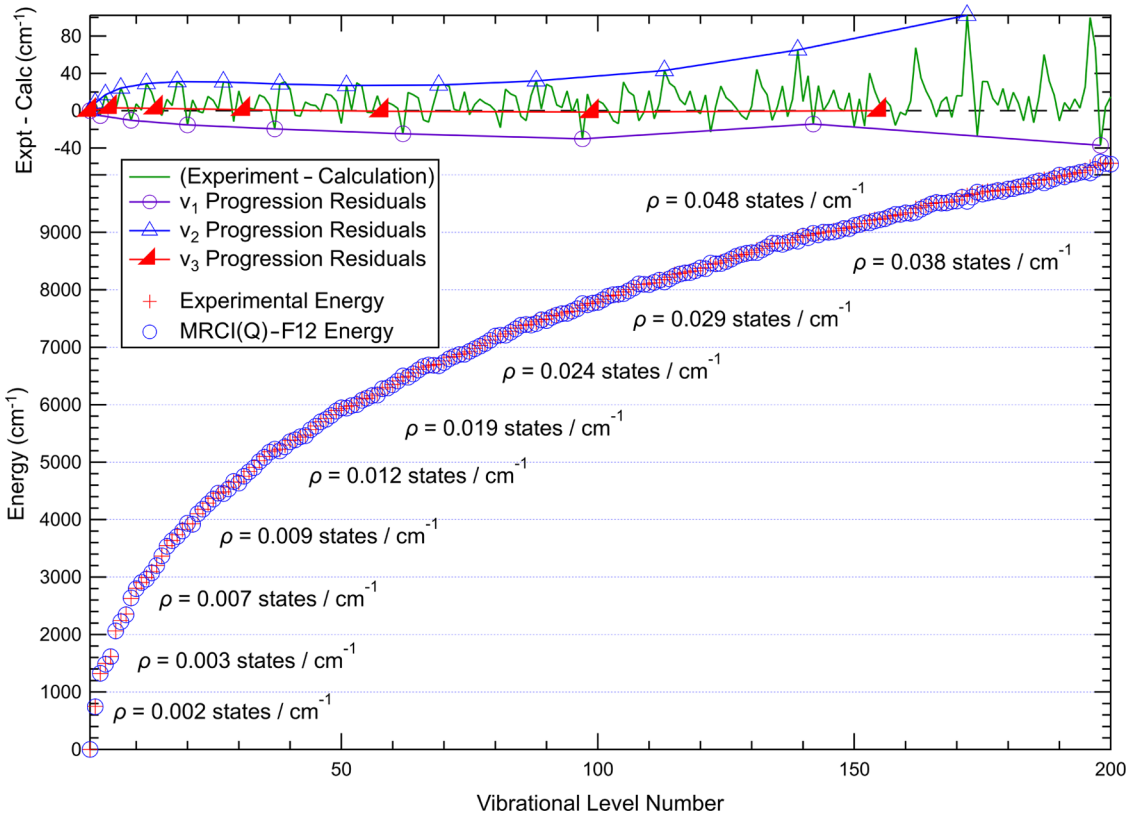

Figure 3. Lowest 200 calculated vibrational levels of the $\tilde{X}$ state (open blue circles) plotted against experimental energies (red crosses) from Delon et al.[16] The green line at the top is the error (expt. − calc.) for each level, highlighting the three (ν_1, ν_2, and ν_3) pure modal progressions. The density of vibrational states (ρ) is also noted in each 1000 cm^{-1} window.

distributions at elevated temperatures, arbitrary weightings can be specified, for example, to simulate transient absorption experiments that create an excited initial state—such as (1,0,1), the target of measurements in this study.

RESULTS AND DISCUSSION

Previously, to help characterize the accuracy of the PESs, we reported a comparison of the lowest 125 vibrational levels on the ground ($\tilde{X}$) electronic state with corresponding experimental

https://doi.org/10.1021/acs.jpca.3c02832
J. Phys. Chem. A 2023, 127, 6051−6062

Table 3. First 100 Rotational Levels of $\tilde{X}$ (0,0,0) Organized in Groups by $N^{a,b}$

level	N_{K_a,K_c}	calc.	expt.	Δ	level	N_{K_a,K_c}	calc.	expt.	Δ
1	$0_{0,0}$	0.000	0.000	0.000	51	$7_{1,7}$	30.858	30.888	0.030
2	$1_{0,1}$	0.842	0.845	0.003	52	$7_{1,6}$	31.502	31.539	0.037
3	$1_{1,1}$	8.460	8.400	−0.060	53	$7_{2,6}$	54.041	53.916	−0.125
4	$1_{1,0}$	8.483	8.423	−0.060	54	$7_{2,5}$	54.047	53.923	−0.124
5	$2_{0,2}$	2.524	2.534	0.010	55	$7_{3,5}$	92.032	91.649	−0.383
6	$2_{1,2}$	10.119	10.070	−0.049	56	$7_{3,4}$	92.032	91.649	−0.383
7	$2_{1,1}$	10.188	10.139	−0.049	57	$7_{4,4}$	144.992	144.253	−0.739
8	$2_{2,1}$	33.010	32.779	−0.231	58	$7_{4,3}$	144.992	144.253	−0.739
9	$2_{2,0}$	33.010	32.779	−0.231	59	$7_{5,3}$	212.702	211.521	−1.181
10	$3_{0,3}$	5.047	5.066	0.019	60	$7_{5,2}$	212.702	211.521	−1.181
11	$3_{1,3}$	12.608	12.571	−0.037	61	$7_{6,2}$	294.895	293.198	−1.697
12	$3_{1,2}$	12.746	12.710	−0.036	62	$7_{6,1}$	294.895	293.198	−1.697
13	$3_{2,2}$	35.534	35.331	−0.203	63	$7_{7,1}$	391.258	388.993	−2.265
14	$3_{2,1}$	35.534	35.332	−0.202	64	$7_{7,0}$	391.258	388.993	−2.265
15	$3_{3,1}$	73.521	73.037	−0.484	65	$8_{0,8}$	30.320	30.378	0.058
16	$3_{3,0}$	73.521	73.037	−0.484	66	$8_{1,8}$	37.547	37.548	0.001
17	$4_{0,4}$	8.410	8.442	0.032	67	$8_{1,7}$	38.373	38.384	0.011
18	$4_{1,4}$	15.926	15.903	−0.023	68	$8_{2,7}$	60.821	60.670	−0.151
19	$4_{1,3}$	16.156	16.135	−0.021	69	$8_{2,6}$	60.833	60.681	−0.152
20	$4_{2,3}$	38.899	38.715	−0.184	70	$8_{3,6}$	98.815	98.407	−0.408
21	$4_{2,2}$	38.899	38.716	−0.183	71	$8_{3,5}$	98.817	98.407	−0.410
22	$4_{3,2}$	76.885	76.434	−0.451	72	$8_{4,5}$	151.727	151.014	−0.713
23	$4_{3,1}$	76.885	76.434	−0.451	73	$8_{4,4}$	151.779	151.014	−0.765
24	$4_{4,1}$	129.839	129.017	−0.822	74	$8_{5,4}$	219.439	218.287	−1.152
25	$4_{4,0}$	129.839	129.017	−0.822	75	$8_{5,3}$	219.439	218.287	−1.152
26	$5_{0,5}$	12.614	12.662	0.048	76	$8_{6,3}$	301.635	299.970	−1.665
27	$5_{1,5}$	20.074	20.066	−0.008	77	$8_{6,2}$	301.635	299.970	−1.665
28	$5_{1,4}$	20.418	20.414	−0.004	78	$8_{7,2}$	398.001	395.774	−2.227
29	$5_{2,4}$	43.104	42.939	−0.165	79	$8_{7,1}$	398.001	395.774	−2.227
30	$5_{2,3}$	43.106	42.941	−0.165	80	$8_{8,1}$	508.190	505.393	−2.797
31	$5_{3,3}$	81.092	80.664	−0.428	81	$8_{8,0}$	508.190	505.393	−2.797
32	$5_{3,2}$	81.092	80.664	−0.428	82	$9_{0,9}$	37.882	37.968	0.086
33	$5_{4,2}$	134.048	133.258	−0.790	83	$9_{1,9}$	45.011	45.039	0.028
34	$5_{4,1}$	134.048	133.258	−0.790	84	$9_{1,8}$	46.044	46.083	0.039
35	$5_{5,1}$	201.754	200.511	−1.243	85	$9_{2,8}$	68.391	68.268	−0.123
36	$5_{5,0}$	201.754	200.511	−1.243	86	$9_{2,7}$	68.408	68.285	−0.123
37	$6_{0,6}$	17.659	17.725	0.066	87	$9_{3,7}$	106.390	106.008	−0.382
38	$6_{1,6}$	25.051	25.061	0.010	88	$9_{3,6}$	106.390	106.008	−0.382
39	$6_{1,5}$	25.534	25.549	0.015	89	$9_{4,6}$	159.354	158.618	−0.736
40	$6_{2,5}$	48.151	48.006	−0.145	90	$9_{4,5}$	159.354	158.618	−0.736
41	$6_{2,4}$	48.155	48.010	−0.145	91	$9_{5,5}$	227.071	225.895	−1.176
42	$6_{3,4}$	86.141	85.735	−0.406	92	$9_{5,4}$	227.071	225.895	−1.176
43	$6_{3,3}$	86.142	85.735	−0.407	93	$9_{6,4}$	309.273	307.584	−1.689
44	$6_{4,3}$	139.098	138.335	−0.763	94	$9_{6,3}$	309.273	307.584	−1.689
45	$6_{4,2}$	139.099	138.335	−0.764	95	$9_{7,3}$	405.645	403.395	−2.250
46	$6_{5,2}$	206.806	205.597	−1.209	96	$9_{7,2}$	405.645	403.395	−2.250
47	$6_{5,1}$	206.807	205.597	−1.210	97	$9_{8,2}$	515.781	513.023	−2.758
48	$6_{6,1}$	288.997	287.265	−1.732	98	$9_{8,1}$	515.839	513.023	−2.816
49	$6_{6,0}$	288.998	287.265	−1.733	99	$9_{9,1}$	639.419	636.162	−3.257
50	$7_{0,7}$	23.544	23.630	0.086	100	$9_{9,0}$	639.420	636.162	−3.258

[a]The calculated (calc.) levels produced using MCTDH and our PES are compared with levels derived from reported constants fitted to experimental (expt.) measurements[23,24] (Δ = expt − calc). The experimental levels are averaged over small fine and hyperfine splittings that are neglected in our calculations (see text). All energies are in cm^{-1}. [b]The RMSE over all 100 levels (extending above 600 cm^{-1} in energy) is only 1.14 cm^{-1}, while the average percentage error is 0.44%.

measurements.[1] The root-mean-square error (RMSE) obtained for that set was 16.53 cm^{-1}, and by tracking the error for each modal progression, it was observed that the errors do not increase dramatically with energy. Here, to provide more initial states for the finite temperature absorption spectrum calculations, we extended those calculations to include the lowest 200 vibrational levels. Evaluation of the partition function at 2800 K indicates that inclusion of 200 levels accounts for 98% of the total weight at that temperature. The extended list of vibrational levels is included in the SI. The close correspondence between

https://doi.org/10.1021/acs.jpca.3c02832
J. Phys. Chem. A 2023, 127, 6051−6062

the calculated and experimentally measured levels is plotted in Figure 3—as well as each modal progression residual and the density of states with energy. The biggest discrepancies are for states with many quanta in the bending mode, with the error reaching 102 cm^{-1} for the (0,13,0) state. Nevertheless, overall, upon extending the number of levels in the set from 125 to 200, the total RMSE only increased slightly, from 16.53 to 21.86 cm^{-1}. No discrepancies in modal character (assignments) or missing states were noted within these 200 levels.

Although vibrational levels are most sensitive to the shape of the well or wells in the PES, for a semirigid molecule, rotational levels depend primarily on the equilibrium structure (which provides the rotational constants, three in the case of an asymmetric top) and secondarily on the shape of the PES (which provides higher-order contributions such as centrifugal distortion). However, as described above, we compute the rotational states using the MCTDH approach rather than from an effective Hamiltonian model. This means that using MCTDH—with a numerically exact kinetic energy operator—and our PES, the rotational levels are directly obtained variationally, in groups according to the specified value of quantum number N. Since our PES yields both an accurate equilibrium structure (reported previously[1]) and an accurate well shape (evidenced by the accuracy of the predicted vibrational levels), not surprisingly the computed rotational levels are in close agreement with experiments (*cf.* Table 3). A number of experimental studies beginning in the 1960s derived and reported molecular parameters, including rotational constants and several orders of distortion, hyperfine, and electron spin-rotation parameters.[23−26] In 1981, Brown et al. reported A, B, and C rotational constants, slightly refined over earlier derivations.[24] Their values of A = 239.90460 GHz, B = 13.002176 GHz, and C = 12.304816 GHz are closely matched by the values we obtain by fitting our lowest few computed levels: A = 241.34792 GHz, B = 12.96602 GHz, and C = 12.27650 GHz. Errors in our fitted constants are all below 1% (0.60, 0.28, and 0.23% for A, B, and C, respectively).

In our calculations, we neglect the $S = 1/2$ spin term for two reasons. First, the spin-rotation coupling is small in this system.[23,24] Second, no spin-changing transitions have been observed. Indeed, all observed transitions satisfy $\Delta J = \Delta N$ such that two separate, very similar manifolds are recorded—denoted the negative and positive branches.[23] Thus, neglecting the electron spin, we approximate $J = N$, and for the temperature-dependent absorption spectra, we refer to the rotational levels in terms of N. Nevertheless, in order to benchmark the PES and the MCTDH approach to computing levels, as well as to appreciate the energy structure of the rotational levels, we present the first 100 levels in Table 3 grouped by N. The experimentally derived levels were produced using the constants reported by Brown et al.[24] and the SPFIT package.[27−29] As seen in the table, for each value of N, there is a progression in energy from the lowest level, which has $K_a = 0$ and $K_c = N$, up to the highest level, which has $K_a = N$ and $K_c = 0$. Since we neglect the electron spin-rotation coupling and nuclear ^{14}N hyperfine splitting, the experimentally derived levels given in the table were averaged over the detailed split levels. The pure *ab initio* approach using MCTDH does remarkably well at reproducing the level structure. There are no anomalies or outliers. The magnitude of error in the calculated levels is largest for the highest energy levels, those above 600 cm^{-1}, but the relative error remains small. The average percentage error over all 100 levels is 0.44%, while the RMSE is 1.14 cm^{-1}.

We separately assessed two contributions—rotational and vibrational excitation—for their effects due to thermal excitation on the electronic absorption spectrum. This was done using a Boltzmann weighting of hundreds of individual spectral contributions, each representing a different thermally populated initial state. The reason that highly vibrationally excited states were explored separately is due to the extremely large number of rovibrational states that become involved at high energies. While large sets of line lists have been assembled for some molecules, it would be an enormous effort to generate and process electronic spectra corresponding to each initial rovibrational state populated at, for example, 1000 K. Analysis of the rotational partition function finds that thousands of states from more than 300 levels contribute significantly even at temperatures as low as 70 K. This is because for each N, there are $2N + 1$ levels (see Table 3), and each of those levels corresponds in turn to $2N + 1$ degenerate states.

The Spectral Simulation Tool described above was used to process the data, apply weights determined from the partition functions, and render comparisons with experimental data sets. As shown in Figures 4 and 5, created with the tool, the

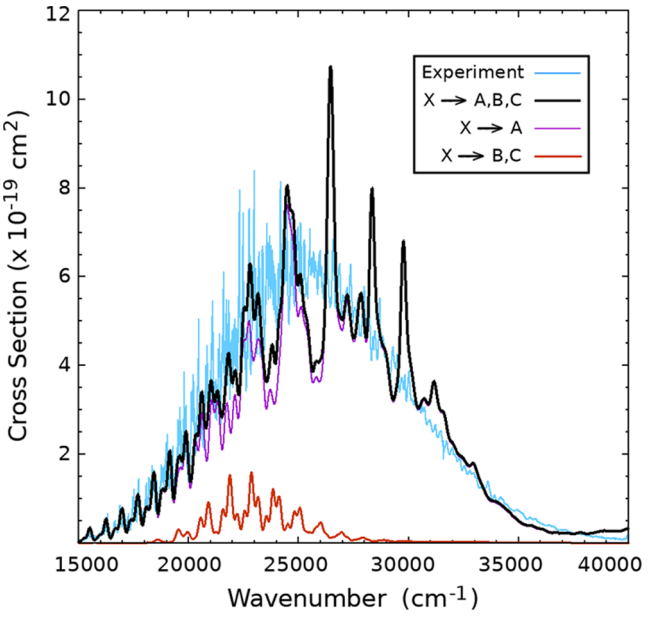

Figure 4. Calculated electronic absorption spectrum from a thermal distribution of rotationally excited initial states at 70 K is compared with an experiment performed by Vandaele et al.[2] at 294 K. At 70 K, more than 300 individual spectra (corresponding to different initial rotational states, not including degeneracy, up to $N_{max} = 20$) contribute to the spectrum. See the text for details.

differences between the 0 and 70 K predictions are fairly subtle at the resolution of the simulated spectra. Nevertheless, especially in the low-energy wing of the spectrum (see Figure 5, left), a slight shift in the envelope and in the relative intensity of peaks within the detailed structure brings the 70 K prediction closer to that of the high-resolution 294 K measurement by Vandaele et al.[2] Perhaps even better agreement is found with the detailed structure in the lower-resolution measurements made by Bogumil et al.[30] at 203 K (see Figure 5, right). Given the modest impact of including rotationally excited states—and their sheer number—this approach was not extended to the many thousands of states that are relevant in a direct comparison at 294 K.

https://doi.org/10.1021/acs.jpca.3c02832
J. Phys. Chem. A 2023, 127, 6051−6062

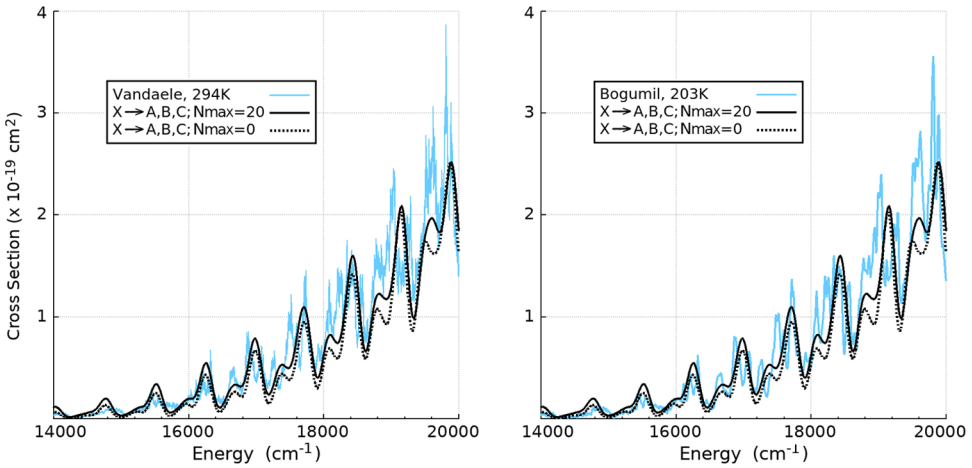

Figure 5. (Left) Calculated electronic absorption spectrum weighting rotationally excited initial states at 70 K (up to $N_{max} = 20$) improves agreement with the 294 K experimental spectrum of Vandaele et al.[2] compared to a 0 K ($N_{max} = 0$) calculation. There is also improved agreement between the 70 K calculation and the lower-resolution 203 K measurement of Bogumil et al.[30] (right).

The effects of temperature on the absorption spectrum of NO_2 were considered previously by Kirmse et al.[22] from an empirical standpoint. They parameterized a model for shifts in the gross spectral envelope for temperatures between 200 and 600 K, focusing on the low-energy side of the spectrum. Experimental uncertainties due to photodissociation and a temperature-dependent equilibrium with N_2O_4 were cited as reasons to exclude the high-energy side of the spectrum from their model. The high-energy side appeared to be less affected by temperature in any case. The main effects discussed by Kirmse et al. are smoothing of the detailed structure (due to averaging over individual state contributions) and growth of intensity in the wings of the spectrum (due to spreading of the initial probability density). We implemented their model for reproducing the envelope and compare it in Figure 6 to our calculations at 200 and 600 K. Their model was constructed as an accurate fit to available data, whereas our prediction is that of unadjusted absolute intensity derived using the transition dipole moment surfaces. The calculated spectral profile agrees well with the model, both in the intensity of the envelope and in the degree of temperature-induced shift in this range.

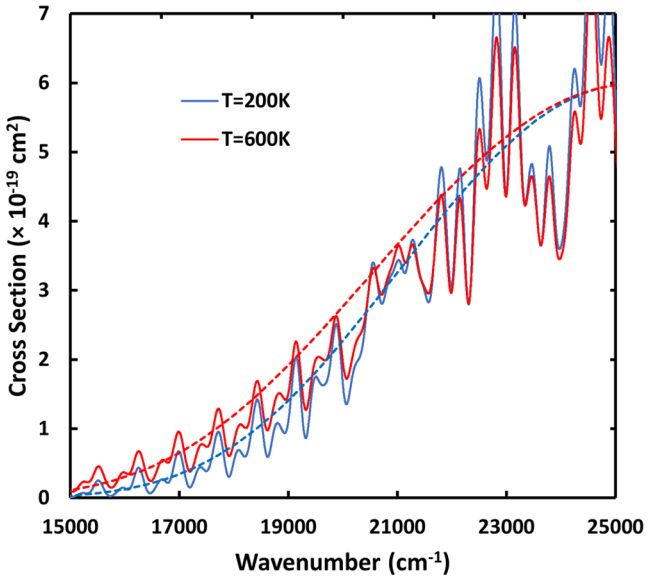

Figure 6. Effect of temperature on the gross spectral envelope in the range of 200−600 K is described by comparing the low-energy wing of the predicted (solid lines) absorption spectrum with the empirical model (dashed lines) proposed by Kirmse et al.[22]

An important feature of the model by Kirmse et al. (that confines its applicability to the 200−600 K range for which it was designed) is the fact that the intensity is held constant at the maximum of the spectrum—notice that the two traces of the model shown in Figure 6 converge at the right edge of the plot. This approximation is inconsistent with the expected behavior at higher temperatures, where vibrationally excited states become relevant. Indeed, the probability densities of vibrationally excited states spread much more dramatically, and a nodal structure is also introduced. For thermal excitation, the ground vibrational state is always the most populated, but as temperature increases, population is transferred into higher energy vibrational levels, whose state density also increases with increasing energy (see Figure 3). The net result is a substantial drop in intensity at the maximum and spreading (growth of the wings) of the spectrum, especially on the low-energy side. Figure 7 plots predicted spectra at a sequence of elevated temperatures reaching 2200 K.

Measurements of part of the absorption cross section at two significantly elevated temperatures (669 and 1313 K) were reported in 1976 by Paulsen and Huffman,[31] and allow us to validate our predictions. As seen in Figure 8, our calculations closely match those results at both temperatures, including the significant drop in intensity at the absorption maximum that was not included in the temperature-dependent model of Kirmse et al. In the figure, we present both the direct $N = 0$ calculation and a smoothed version that better matches the experimental envelope.

In 2002, Liu et al.[32] reported measurements in a shock tube of the temperature-dependent absorption cross section to even higher temperatures, but only for a single wavelength, 390.130 nm (25,633 cm^{-1}), near the absorption maximum. This single-wavelength experiment makes comparison with our calculations slightly more difficult because our predicted spectrum for $N = 0$ is quite oscillatory and the comparison depends on whether the experimentally probed frequency is on a peak or trough. Thus, in Figure 9, we also compare results derived from the smoothed envelope. The smoothed calculation agrees quite well with the reported measurements, being just below the experimental uncertainty from 300 to 600 K, within experimental uncertainty

https://doi.org/10.1021/acs.jpca.3c02832
J. Phys. Chem. A 2023, 127, 6051−6062

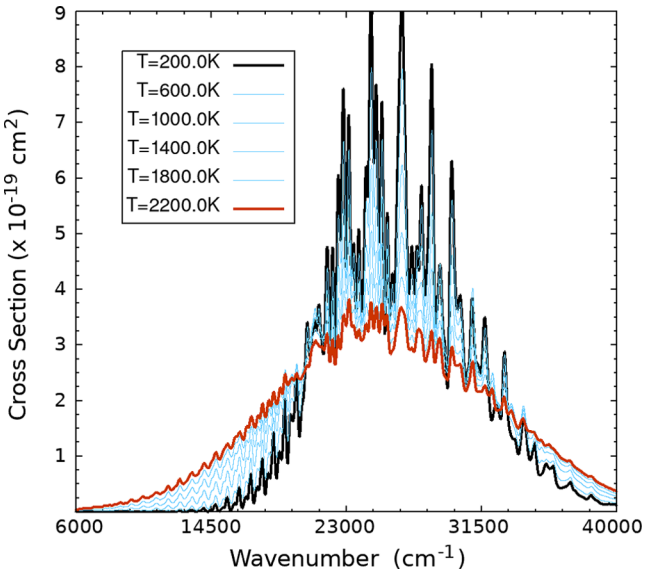

Figure 7. The Spectral Simulation Tool was used to yield predicted spectra due to vibrational excitation at a sequence of temperatures.

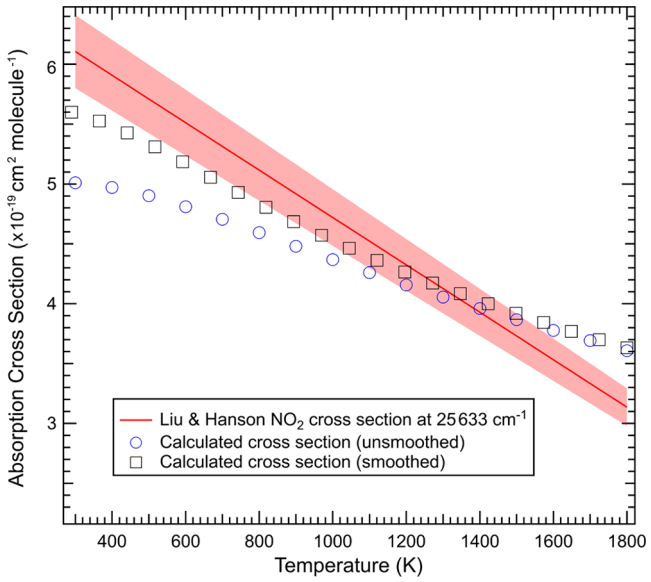

Figure 9. Measurements of the absorption cross section (red, with shaded uncertainty) vs temperature at a single wavelength are compared with the raw $N = 0$ and smoothed computed spectra for that particular energy (see text).

from 600 to 1500 K, and just above experimental uncertainty for temperatures approaching 1800 K.

At high temperatures in thermal equilibrium, the absorption spectrum is highly averaged over the initial vibrationally excited states. For comparison, we also calculate spectra arising from single excited initial vibrational states—such as might be accessed in transient absorption experiments. Spectra for initial states with one quantum of energy in each mode, the (1,0,0), (0,1,0), and (0,0,1) states, are plotted in Figure 10. Although the impact of vibrational modal excitation on the probability densities of the initial states is simple and easy to predict (several examples are plotted in our previous paper[1]), the impact on the absorption spectrum is much more complicated. It depends on the relationship between the ground- and excited-electronic-state topographies and is further modulated by the transition dipole surfaces. Some plots of the PESs and transition dipole surfaces are given in the SI for reference. Perhaps the most remarkable predicted effect on the absorption spectra results from bend excitation on the $\tilde{B}/\tilde{C} \leftarrow \tilde{X}$ transition, as given in Figure 10 (middle).

Figure 11 further explores the effect of bend excitation on the predicted individual spectral contributions up to five quanta.

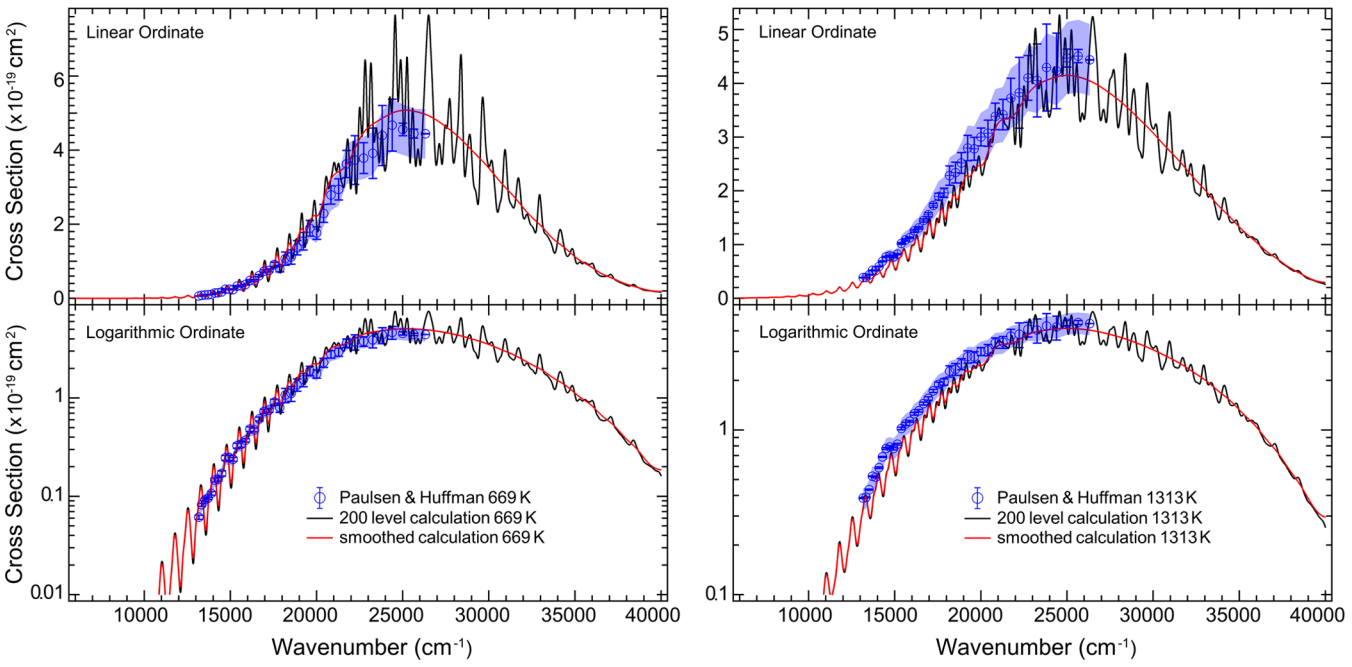

Figure 8. Measurements of part of the absorption spectrum at 669 (left) and 1313 K (right) performed by Paulsen and Huffman in 1976[31] are compared with raw $N = 0$ and smoothed predictions (see text). Statistical uncertainty in the experiments is shown by error bars, whereas the authors' estimation of systematic uncertainty is shown as shaded blue regions.

https://doi.org/10.1021/acs.jpca.3c02832
J. Phys. Chem. A 2023, 127, 6051−6062

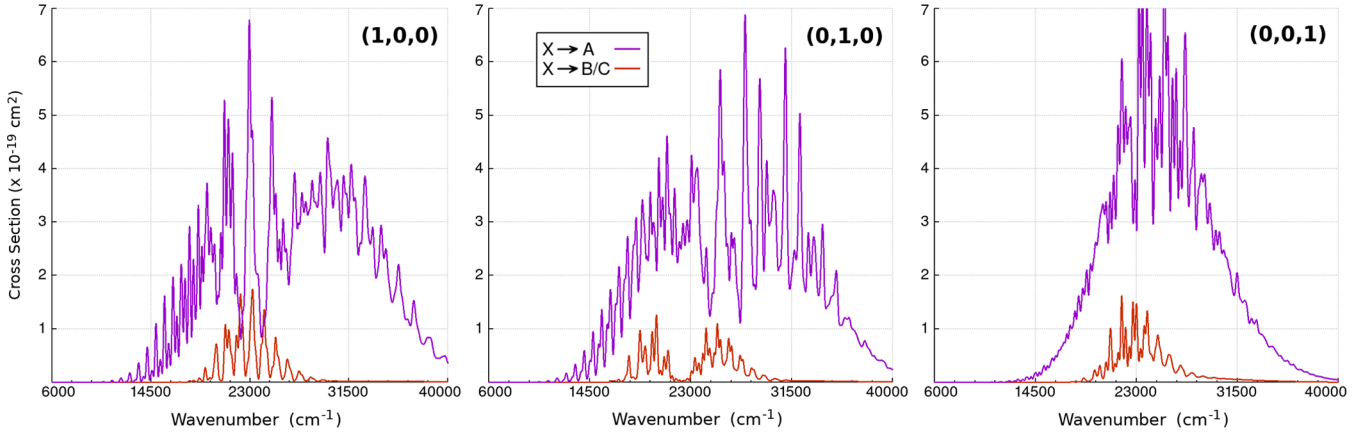

Figure 10. Simulated spectra for one quantum of excitation in the (left) symmetric stretch (1,0,0), (middle) bend (0,1,0), and (right) asymmetric stretch (0,0,1) modes are plotted for $\tilde{A} \leftarrow \tilde{X}$ (purple trace) and $\tilde{B}/\tilde{C} \leftarrow \tilde{X}$ (red trace). For (0,1,0) the $\tilde{B}/\tilde{C} \leftarrow \tilde{X}$ contribution exhibits the nodal pattern of the initial probability density cleanly projected onto the spectrum (see text).

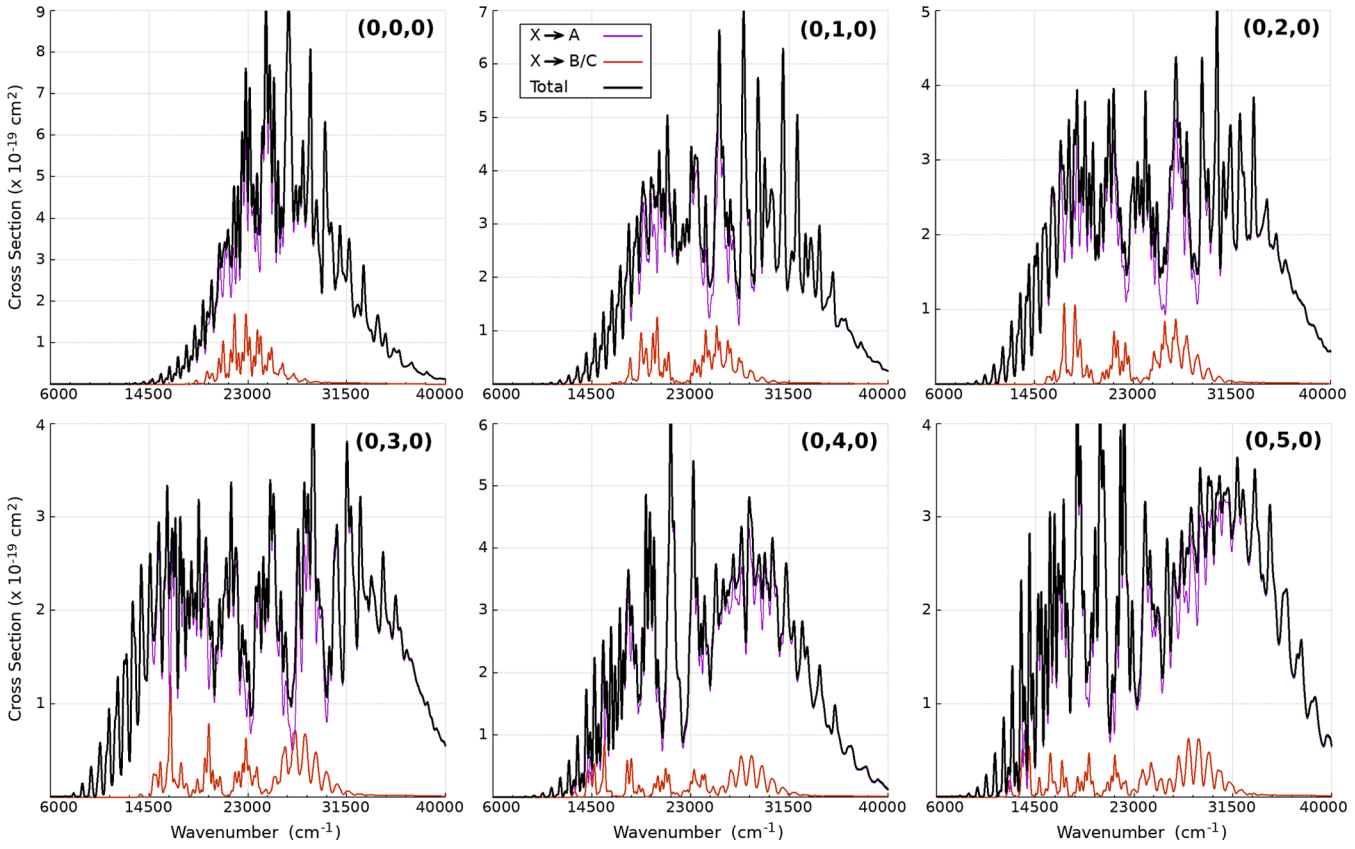

Figure 11. Projection of the nodal pattern from the probability density of the initial state, noted in Figure 10, is explored for up to 5 bend quanta and is found to persist, especially for the $\tilde{B}/\tilde{C} \leftarrow \tilde{X}$ contribution.

With bend excitation, the vibrational probability distribution on the ground $\tilde{X}$ state exhibits nodes in the angular coordinate. The energy of the bright $\tilde{B}$ state above has a roughly linear dependence on the bond angle for small displacements in this range. Thus, rather intuitively (such as via the reflection principle), the result is a spectrum that is a clear projection of the initial state probability density, complete with nodal structure. Note also that the energetic range of the $\tilde{B}/\tilde{C} \leftarrow \tilde{X}$ spectral contribution changes more rapidly with increasing bend excitation on the low-energy side of the spectrum compared to the high-energy side. On the other hand, even for the (0,1,0) initial state, the effects in nodal structure and energetic limits on the $\tilde{A} \leftarrow \tilde{X}$ contribution are entirely different, due to the $\tilde{A}$ state having a less favorable topography for a clean projection. Remarkably, even up to five quanta, the nodal pattern observed in the $\tilde{B}/\tilde{C} \leftarrow \tilde{X}$ contribution retains a clear signature of the initial state probability density throughout.

It would be valuable to validate our theoretical approach to experimental data at even higher temperatures. Although temperatures above 2000 K can be achieved in shock tube measurements, as pointed out by Liu et al.,[32] the rate of NO_2 thermal decomposition is too great at these temperatures to perform direct absorption spectroscopy. As another approach for validation, we performed a transient absorption experiment

https://doi.org/10.1021/acs.jpca.3c02832
J. Phys. Chem. A 2023, 127, 6051−6062

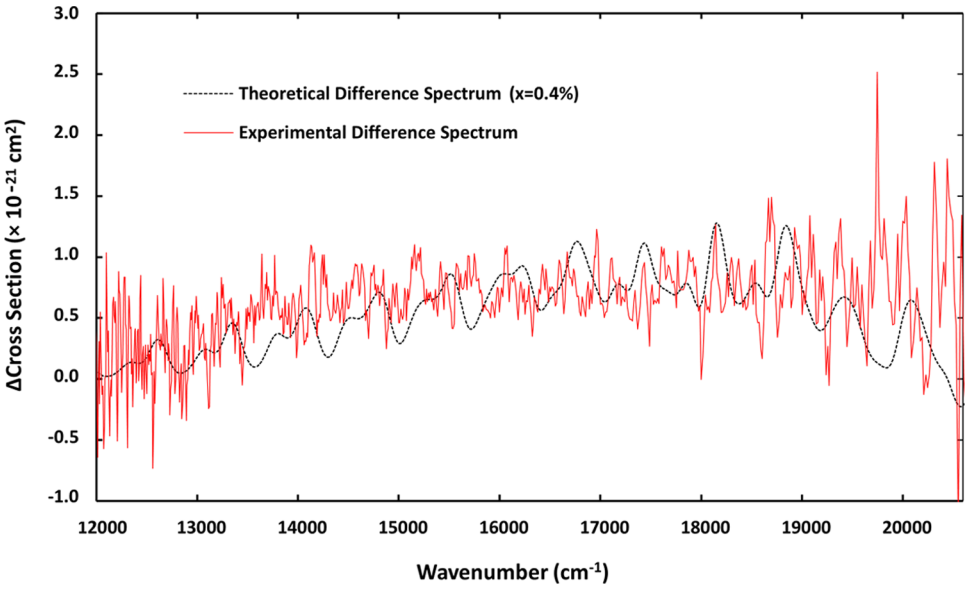

Figure 12. Comparison of the experimental difference spectrum after (1,0,1) overtone excitation (red) with the corresponding theoretical difference spectrum (dashed black) at an excitation fraction of 0.4%.

to probe how the population of the (1,0,1) vibrational level modifies the electronic absorption spectrum. The band origin of the (1,0,1) level is 2906.07 cm^{-1}, which from the Equipartition Theorem corresponds to a temperature of $T = E_{vib}/k_B = 4180$ K. Details of the approach and analysis are given in the SI. Unfortunately, we were unable to experimentally determine the fraction of population transfer to the (1,0,1) vibrational level by the infrared OPO pulse, and hence cannot directly extract the electronic spectrum originating purely from the (1,0,1) level. Instead, we measure an experimental difference spectrum with and without OPO excitation, $\Delta\sigma_{expt}$, which is shown in Figure 12. By scaling the theoretical difference spectrum to experiment, we determine an OPO-induced fractional excitation to the (1,0,1) level of 0.4%. Fortunately, the shape of the difference spectrum is independent of this fractional population transfer to the (1,0,1) level. The fact that the shape of the theoretical difference spectrum agrees with the shape of the experimental difference spectrum (to within experimental scatter) provides additional validation of the theoretical approach at higher temperatures.

Finally, we explore the effect of significantly elevated temperatures on the total integrated spectral intensity. We have noted the effects of smoothing, spreading, and lowering of the peak maximum with increasing temperature. If the transition dipole surfaces were constant, independent of changes in bond length and bond angle, then all of those effects would occur without impacting the total integrated spectral intensity. However, as seen in plots given in the SI, although the transition dipole surfaces near the equilibrium geometry are nearly maximal and slowly varying, they decrease significantly with larger nuclear displacement. Thus, for moderate temperatures (up to around 1000 K), the integrated intensity drops only slightly. Given that a drop in this range on the integrated intensity is within their experimental uncertainties, this effect was not included in the model by Kirmse et al.[22] For higher temperatures exceeding 2000 K, the drop-off is much more significant and constitutes an essential aspect of an accurate absolute intensity prediction at high temperatures. As seen in Figure 13, the drop-off with increasing temperature is gradual at

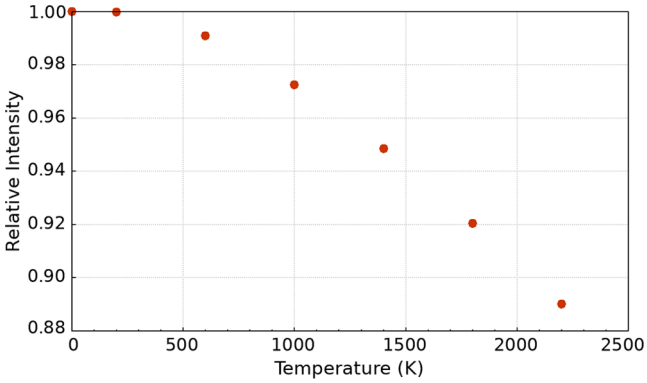

Figure 13. Total spectral intensity integrated from 6000 to 40,000 cm^{-1} as a function of temperature. The data is normalized to the integral at 0 K.

first, still retaining 97% of the 0 K intensity at 1000 K, with a steeper, nearly linear drop above 1000 K. This observation highlights the importance of a first-principles theoretical treatment that does not assume a constant transition dipole moment when accurate cross sections are needed at high temperatures.

CONCLUSIONS AND OUTLOOK

We have extended our theoretical investigation of the electronic absorption spectrum of NO_2 to consider the effects of finite temperature. A direct first-principles approach was undertaken in which hundreds of individual spectra were computed, each corresponding to a different thermally accessible initial state. A Spectral Simulation Tool was developed to process and manage the data. The tool applies weights determined from partition functions—evaluated by direct summation over the levels—and renders spectral plots for any selected temperature.

The absolute intensity of the predicted spectrum was validated over the 200−600 K range in comparison to an empirical model by Kirmse et al. With increased temperature in this range, smoothing (due to averaging) and a slight spreading of the envelope (due to delocalization of the initial wavepacket)

https://doi.org/10.1021/acs.jpca.3c02832
J. Phys. Chem. A 2023, 127, 6051−6062

are observed and well reproduced by our predictions. Pushing our predictions to much higher temperatures (beyond 2000 K), vibrationally excited states comprise a significant portion of the total population. These states cause a more dramatic spreading of the spectral envelope and a corresponding drop in the peak maximum. This evolution is expected because the initial wavepacket probability density is normalized, and excited vibrational states contribute nodal structure. Our high-temperature predictions closely match reported measurements of partial spectra from Paulsen and Huffman at 669 and 1313 K, and those by Liu et al. acquired over a wider temperature range for a single wavelength. Our predicted spectrum for the (1,0,1) initial state was validated via a new transient absorption measurement. We also predict that the total integrated spectral intensity drops off increasingly as a function of temperature due to the shape of the transition dipole moment surfaces, which drop in magnitude away from equilibrium.

In this study, we included 200 vibrational levels, reaching about 10,200 cm^{-1} above the zero point energy, near the minimum of the $\tilde{A}$ state to which the $\tilde{X}$ state is coupled. The density of vibrational states on the $\tilde{X}$ state is quite high in this region, but of course, the $\tilde{A}$ state levels, some known to be perturbed via the coupling, are sparse. In a future paper, we will report calculations of additional levels, extending into the $\tilde{A}$ state manifold, exploring the effects of the coupling as exhibited in perturbed levels and mixed states. Electronic spectra for initial $\tilde{A}$- or mixed-state levels will contribute differently since they are governed by different operators.

■ ASSOCIATED CONTENT

Supporting Information

The Supporting Information is available free of charge at https://pubs.acs.org/doi/10.1021/acs.jpca.3c02832.

Experimental details and analysis procedure for transient absorption experiments; extended list of 200 vibrational levels; and plots of PESs and transition dipole surfaces (PDF)

■ AUTHOR INFORMATION

Corresponding Authors

Richard Dawes − *Missouri University of Science and Technology, Rolla, Missouri 65409-0010, United States;* orcid.org/0000-0002-2493-4671; Email: dawesr@mst.edu

David L. Osborn − *Combustion Research Facility, Sandia National Laboratories, Livermore, California 94551, United States; Department of Chemical Engineering, University of California, Davis, California 95616, United States;* orcid.org/0000-0003-4304-8218; Email: dlosbor@sandia.gov

Authors

Steve Ndengué − *ICTP-East African Institute for Fundamental Research, University of Rwanda, Kigali 4285, Rwanda*

Ernesto Quintas-Sánchez − *Missouri University of Science and Technology, Rolla, Missouri 65409-0010, United States;* orcid.org/0000-0002-4378-8745

Christopher C. Blackstone − *Combustion Research Facility, Sandia National Laboratories, Livermore, California 94551, United States*

Complete contact information is available at: https://pubs.acs.org/10.1021/acs.jpca.3c02832

Notes

The authors declare no competing financial interest.

■ ACKNOWLEDGMENTS

R.D. is supported by the U.S. Department of Energy (Award DE-SC0019740). R.D. thanks professor Garry Grubbs for help with the SPFIT program. Computing resources were supported by the National Science Foundation under Grant No. OAC-1919789. S.N., E.Q.S., C.B., and D.L.O. are supported by the Air Force Technical Applications Center. Sandia National Laboratories is a multimission laboratory managed and operated by National Technology and Engineering Solutions of Sandia, LLC, a wholly owned subsidiary of Honeywell International, Inc., for the USDOE's National Nuclear Security Administration under contract DE-NA0003525. This paper describes objective technical results and analysis. Any subjective views or opinions that might be expressed in the paper do not necessarily represent the views of the USDOE or the US Government.

■ REFERENCES

(1) Ndengué, S.; Quintas-Sánchez, E.; Dawes, R.; Osborn, D. The Low-Lying Electronic States of NO_2: Potential Energy and Dipole Surfaces, Bound States, and Electronic Absorption Spectrum. *J. Phys. Chem. A* **2021**, *125*, 5519−5533.

(2) Vandaele, A. C.; Hermans, C.; Simon, P. C.; Carleer, M.; Colin, R.; Fally, S.; Merienne, M.-F.; Jenouvrier, A.; Coquart, B. Measurements of the NO_2 absorption cross-section from 42000 cm^{-1} to 10000 cm^{-1} (238−1000 nm) at 220 K and 294 K. *J. Quant. Spectrosc. Radiat. Transfer* **1998**, *59*, 171−184.

(3) Meyer, H. D.; Gatti, F.; Worth, G. A. *Multidimensional Quantum Dynamics: MCTDH Theory and Applications*; Wiley-VCH: Weinheim, 2009.

(4) Beck, M. H.; Jäckle, A.; Worth, G. A.; Meyer, H. D. The multiconfiguration time-dependent Hartree (MCTDH) method: a highly efficient algorithm for propagating wavepackets. *Phys. Rep.* **2000**, *324*, 1−105.

(5) Manthe, U.; Meyer, H.-D.; Cederbaum, L. Multiconfigurational time-dependent Hartree study of complex dynamics: Photodissociation of NO_2. *J. Chem. Phys.* **1992**, *97*, 9062−9071.

(6) Ndengué, S. A.; Gatti, F.; Schinke, R.; Meyer, H.-D.; Jost, R. Absorption cross section of ozone Isotopologues calculated with the multiconfiguration time-dependent Hartree (MCTDH) method: I. The Hartley and Huggins bands. *J. Phys. Chem. A* **2010**, *114*, 9855−9863.

(7) Ndengué, S. A.; Schinke, R.; Gatti, F.; Meyer, H.-D.; Jost, R. Ozone photodissociation: isotopic and electronic branching ratios for symmetric and asymmetric isotopologues. *J. Phys. Chem. A* **2012**, *116*, 12271−12279.

(8) Ndengué, S. A.; Schinke, R.; Gatti, F.; Meyer, H.-D.; Jost, R. Comparison of the Huggins band for six ozone isotopologues: vibrational levels and absorption cross section. *J. Phys. Chem. A* **2012**, *116*, 12260−12270.

(9) Ndengué, S. A.; Dawes, R.; Guo, H. A new set of potential energy surfaces for HCO: Influence of Renner-Teller coupling on the bound and resonance vibrational states. *J. Chem. Phys.* **2016**, *144*, No. 244301.

(10) Worth, G.; Beck, M.; Jäckle, A.; Meyer, H. D. *The MCTDH Package, Version 8.2,(2000), University of Heidelberg, Heidelberg, Germany. H.-D. Meyer, Version 8.3(2002), Version 8.4 (2007), O. Vendrell and H.-D. Meyer, Version 8.5 (2011)*, 2007 http://mctdh.uni-hd.de. (accessed June 07, 2023).

(11) Jäckle, A.; Meyer, H. D. Product representation of potential energy surfaces. *J. Chem. Phys.* **1996**, *104*, 7974−7984.

(12) Jäckle, A.; Meyer, H. D. Product representation of potential energy surfaces. II. *J. Chem. Phys.* **1998**, *109*, 3772−3779.

(13) Doriol, L. J.; Gatti, F.; Iung, C.; Meyer, H.-D. Computation of vibrational energy levels and eigenstates of fluoroform using the

multiconfiguration time-dependent Hartree method. *J. Chem. Phys.* **2008**, *129*, No. 224109.
(14) Meyer, H. D.; Worth, G. A. Quantum molecular dynamics: propagating wavepackets and density operators using the multi-configuration time-dependent Hartree method. *Theor. Chem. Acc.* **2003**, *109*, 251−267.
(15) Meyer, H. D.; Quéré, F. L.; Léonard, C.; Gatti, F. Calculation and selective population of vibrational levels with the Multiconfiguration Time-Dependent Hartree (MCTDH) algorithm. *Chem. Phys.* **2006**, *329*, 179−192.
(16) Delon, A.; Jost, R. Laser induced dispersed fluorescence spectra of jet cooled NO_2: The complete set of vibrational levels up to 10000 cm^{-1} and the onset of the $\tilde{X}^2A_1-\tilde{A}^2B_2$ vibronic interaction. *J. Chem. Phys.* **1991**, *95*, 5686−5700.
(17) Sutcliffe, B. T.; Tennyson, J. A generalized approach to the calculation of ro-vibrational spectra of triatomic molecules. *Mol. Phys.* **1986**, *58*, 1053−1066.
(18) Gatti, F.; Iung, C.; Chapuisat, X. Vector parametrization of the three-atom problem in quantum mechanics II. Valence vectors. *J. Mol. Struct.: THEOCHEM* **1998**, *430*, 201−208.
(19) Iung, C.; Gatti, F.; Viel, A.; Chapuisat, X. Vector parametrization of the N-atom problem in quantum mechanics with non-orthogonal coordinates. *Phys. Chem. Chem. Phys.* **1999**, *1*, 3377−3385.
(20) Sukiasyan, S.; Meyer, H.-D. On the effect of initial rotation on reactivity. A multi-configuration time-dependent Hartree (MCTDH) wave packet propagation study on the H + D_2 and D + H_2 reactive scattering systems. *J. Phys. Chem. A* **2001**, *105*, 2604−2611.
(21) Malenda, R.; Gatti, F.; Meyer, H.-D.; Talbi, D.; Hickman, A. Comparison of the multi-configuration, time-dependent Hartree (MCTDH) method with the Arthurs and Dalgarno coupled-channel method for rotationally inelastic scattering. *Chem. Phys. Lett.* **2013**, *585*, 184−188.
(22) Kirmse, B.; Delon, A.; Jost, R. NO_2 absorption cross section and its temperature dependence. *J. Geophys. Res.: Atmos.* **1997**, *102*, 16089−16098.
(23) Bird, G.; Hunt, G.; Gebbie, H.; Stone, N. The far-infrared pure rotational spectum of nitrogen dioxide (NO_2). *J. Mol. Spectrosc.* **1970**, *33*, 244−273.
(24) Brown, J.; Steimle, T.; Coles, M.; Curl, R., Jr A determination of the spin-rotation parameters for NO_2 in the X state by microwave−optical double resonance. *J. Chem. Phys.* **1981**, *74*, 3668−3672.
(25) Bird, G. R.; Baird, J. C.; Jache, A. W.; Hodgeson, J. A.; Curl, R., Jr; Kunkle, A. C.; Bransford, J. W.; Rastrup-Andersen, J.; Rosenthal, J. Microwave spectrum of NO_2: fine structure and magnetic coupling. *J. Chem. Phys.* **1964**, *40*, 3378−3390.
(26) Lafferty, W. J.; Sams, R. L. The high resolution infrared spectrum of the $2\nu_2+\nu_3$ and $\nu_1+\nu_2+\nu_3$ bands of $^{14}N^{16}O_2$: Vibration and vibration-rotation constants of the electronic ground state of $^{14}N^{16}O_2$. *J. Mol. Spectrosc.* **1977**, *66*, 478−492.
(27) Pickett, H. M. The fitting and prediction of vibration-rotation spectra with spin interactions. *J. Mol. Spectrosc.* **1991**, *148*, 371−377.
(28) Novick, S. E. A beginner's guide to Pickett's SPCAT/SPFIT. *J. Mol. Spectrosc.* **2016**, *329*, 1−7.
(29) Drouin, B. J. Practical uses of SPFIT. *J. Mol. Spectrosc.* **2017**, *340*, 1−15.
(30) Bogumil, K.; Orphal, J.; Homann, T.; Voigt, S.; Spietz, P.; Fleischmann, O.; Vogel, A.; Hartmann, M.; Kromminga, H.; Bovensmann, H.; et al. Measurements of molecular absorption spectra with the SCIAMACHY pre-flight model: instrument characterization and reference data for atmospheric remote-sensing in the 230−2380 nm region. *J. Photochem. Photobiol., A* **2003**, *157*, 167−184.
(31) Paulsen, D.; Huffman, R. *Nitrogen Dioxide Absorption Coefficients at High Temperatures*, Technical Report; Air Force Geophysics Laboratories USAF: United States, 1976.
(32) Liu, J.; Hanson, R.; Jeffries, J. High-sensitivity absorption diagnostic for NO_2 using a blue diode laser. *J. Quant. Spectrosc. Radiat. Transfer* **2002**, *72*, 655−664.

https://doi.org/10.1021/acs.jpca.3c02832
J. Phys. Chem. A 2023, 127, 6051−6062